ULTRAFAST DYNAMICS IN LIGHT DRIVEN MOLECULAR ROTARY MOTORS PROBED BY FEMTOSECOND STIMULATED RAMAN SCATTERING

Christopher R. Hall[†], Jamie Conyard[†], Ismael A. Heisler[†], Garth Jones[†], James Frost[†], Wesley R. Browne[‡], Ben L. Feringa[§]* and Stephen R. Meech[†]*

[†]School of Chemistry, University of East Anglia, Norwich Research Park, Norwich NR4 7TJ, UK, [‡] Molecular Inorganic Chemistry, Stratingh Institute for Chemistry, University of Groningen, Nijenborgh 4, 9747AG Groningen, The Netherlands, and [§] Synthetic Organic Chemistry, Stratingh Institute for Chemistry, University of Groningen, Nijenborgh 4, 9747AG Groningen, The Netherlands

Abstract

Photochemical isomerization in sterically crowded chiral alkenes is the driving force for molecular rotary motors in nanoscale machines. Here the excited state dynamics and structural evolution of the prototypical light driven rotary motor are followed on the ultrafast timescale by femtosecond stimulated Raman spectroscopy (FSRS) and transient absorption (TA). TA reveals a sub 100 fs blue shift and decay of the Franck-Condon bright state arising from relaxation along the reactive potential energy surface. The decay is accompanied by coherently excited vibrational dynamics which survive the excited state structural evolution. The ultrafast Franck-Condon bright state relaxation is to a dark excited state, which FSRS reveals to have a rich spectrum compared to the electronic ground state, with the most intense Raman active modes shifted to significantly lower wavenumber. This is discussed in terms of a reduced bond order of the central bridging bond and overall weakening of bonds in the dark state, which is supported by electronic structure calculations. The observed evolution in the FSRS spectrum is assigned to vibrational cooling accompanied by partitioning of the dark state between the product isomer and the original ground state. Formation of the product isomer is observed in real time by FSRS. It is formed vibrationally hot and cools over several picoseconds, completing the characterization of the light driven half of the photocycle.

*authors for correspondence (s.meech@uea.ac.uk) and (b.l.feringa@rug.nl).

Introduction

The design and synthesis of molecular machines is a major challenge for chemistry and chemical biology,[1-5] with the stimulation and control of molecular motion at its heart. Power can be delivered to molecular machines both chemically and electrochemically, but the least invasive approach is conversion of light energy to mechanical motion. In the 1990s, Feringa and co-workers developed a family of unidirectional light driven molecular motors based on a chiral sterically crowded alkene core.[4, 6-7] These rotary motors function by successive orthogonal photochemical and thermal steps, where the structure and stereochemistry impose unidirectional rotation about the olefinic bond (Figure 1).[8-10] Their synthetic versatility has opened up numerous opportunities for applications as light driven molecular motors in nanomachines. Successive generations of molecular motors enabled control over the rate determining thermal step and operation at ever higher frequencies (currently exceeding 1 MHz). Recent advances have enabled the chiral centre to be dispensed with;[9, 11-13] several examples have already featured in molecular scale devices.[14-17]

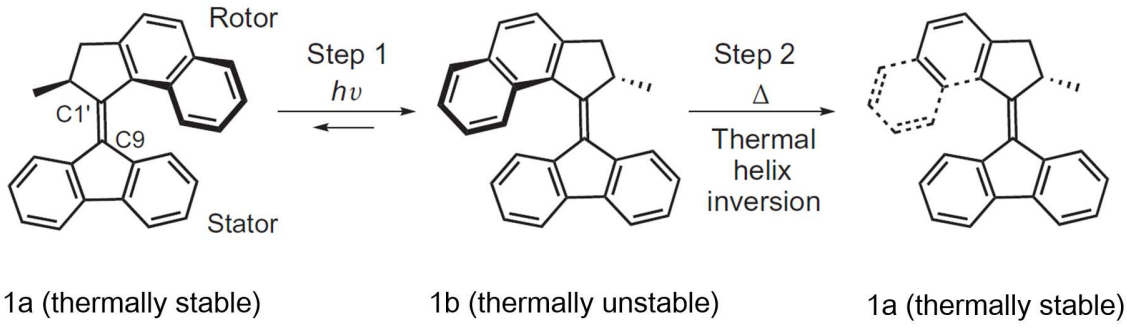

Figure 1. Photomolecular Rotor Photocycle. Absorption of a photon reduces the olefinic bond order giving rise to isomerization of **1a** to yield the metastable ground state **1b**. A second thermally activated step completes the isomerization and reforms the initial ground state. The cycle is then repeated.

Despite the exquisite control achieved over the thermal step of their operation, the lack of synthetic control over the photochemical quantum yield of the power stroke (Figure 1), reduces the motor's efficiency resulting in absorbed energy being dissipated as heat.[9-10] Rational control by design of this step necessitates understanding the excited state dynamics, and how they lead to partitioning between isomerization and unproductive relaxation back to the original ground state. Quantum chemical calculations by Filatov and co-workers determined that excited state pathways for molecular rotors are dependent on accessible conical intersections (CIs) where efficient radiationless decay to the ground state occurs.[18-19] These CIs were characterized by a twist about the central double bond and a strong pyramidalization at one of the olefinic carbon atoms. Populations were calculated yielding a sub-picosecond excited state lifetime and a quantum yield of ca 0.3, in qualitative agreement with experimental observations. Experimentally, Conyard et al. measured excited state dynamics with sub 50 fs resolution time resolved fluorescence and picosecond transient absorption.[20-21] They resolved a biphasic excited state relaxation, with a dominant initial fluorescence decay of <100 fs, which was assigned to excited state structural evolution from a Franck-Condon excited bright state to a dark state on the S_1 potential energy surface. The weak dependence of bright state decay time on solvent viscosity was consistent with motion along a coordinate which does not displace a large solvent volume, such as the pyramidalization coordinate identified in calculations. The S_1 dark state was observed in transient absorption to relax to the S_0 ground state in ca 1.5 ps. The appearance of the 1.5 ps decay as a component in the bright state fluorescence was interpreted as an equilibration between the two states.[20-21] Superimposed on the fluorescence decay were oscillations arising from coherent excitation of vibrational modes in the S_1 state.[20]

Following these early investigations of excited state dynamics, there have been a number of developments in research calculating the temporal evolution of nuclear and electronic structure on the excited state potential energy surface of the prototypical molecular rotor **1a** (Figure 1) and related molecules.[22-28] Some new and potentially more efficient motors have been described.[22, 29-30]

In many of these calculations the nature and structure of the dark state plays a key role, yet remains a topic of debate.[25, 28] Here we combine femtosecond stimulated Raman spectroscopy (FSRS) and transient absorption (TA) experiments with 100 fs time resolution to resolve the excited state structural dynamics of **1a**.[31] These two complementary techniques have been shown to provide high levels of detail in resolving structural dynamics in a number of photochemical and photobiological reactions.[32-35] In particular, resonant FSRS (and its time domain analog[36-40]) provides the time dependent vibrational signature of the resonant transient states.

Applied to **1a**, FSRS yields new experimental insight into molecular structural evolution associated with motor photochemistry. Very recently the first calculations of the vibrational spectrum of the dark excited electronic state of **1a** were reported, and compared with picosecond transient IR data This represents an important first step in characterising dark state structure, but the early time IR spectra were dominated by low lying electronic transitons.[25] Here using FSRS we provide a well resolved Raman spectrum of the dark state between 200 fs and 100 ps after excitation. A feature of resonance enhanced FSRS is that it yields a spectrum unperturbed by ground state bleaches or other sources of transient IR absorption.[41] Thus, these FSRS data provide an essential test of future calculations. The TA data are consistent with earlier fluorescence studies, but detailed analysis of TA and FSRS together reveals an important role for intramolecular vibrational redistribution (IVR) in each photochemical step. Further, the FSRS data characterize the formation of vibrationally hot **1b** from the dark state in real time, while TA data reveal the persistence of vibrational coherence following conversion of the light to dark state.

Results and Discussion.

The TA data for **1a** in cyclohexane (Figure 2A) show two excited state absorptions bands at 760 nm and 550 nm. Within 100 fs the 760 nm transition shifts to higher energy and decays to a nonzero final value. Simultaneously the 550 nm band gains amplitude, reaching a maximum at 120 fs. A more accurate time constant for this primary step cannot be obtained, as it is close to the

instrumental time resolution, but a 100 fs timescale is consistent with time resolved fluorescence studies of **1a**, which had a dominant decay time of 80 fs.[20-21] Thus, the 760 nm TA can be assigned to the fluorescent (bright) Franck-Condon excited state. Beyond 120 fs both bands decay uniformly with a time constant of 1.6±0.2 ps to the baseline, leaving a long lived transient absorbing below 500 nm (Fig. 2). This long lived transient is assigned to formation of **1b**, which has its absorption onset below 500 nm (Fig. S8). As previously noted,[21] **1b** is formed directly as the 1.6 ps excited state intermediate decays; consistent with that, an isosbestic point is observed at 480 nm persisting over the first 1 ps (Fig 2A). The isosbestic point is absent at later times, being replaced by a monotonic decay. The loss of the isosbestic point is ascribed to vibrational cooling in the ground state of **1b**, which is formed from the 550 nm absorbing excited state with considerable excess energy. As the **1b** ground state cools the hot-band contribution to the red edge absorption (ca 480 nm) will decrease, thus modifying the shape of the spectrum.

These TA data are consistent with the previous model developed on the basis of time resolved fluorescence and picosecond TA.[20-21] The newly observed ultrafast decay in the 760 nm TA band is assigned to the short lived bright state. Its decrease in amplitude and blue shift reflects the ultrafast structural distortion as the Frank-Condon excited state evolves towards a dark state, to which the rapidly rising 550 nm TA is assigned. These states establish an equilibrium and decay in parallel with the 1.6 ps decay constant. The dark state partitions via a CI to either the original ground state, **1a**, or the metastable state, **1b**. The principal conclusions concerning population dynamics on the excited state potential surface are summarized in Figure 3.

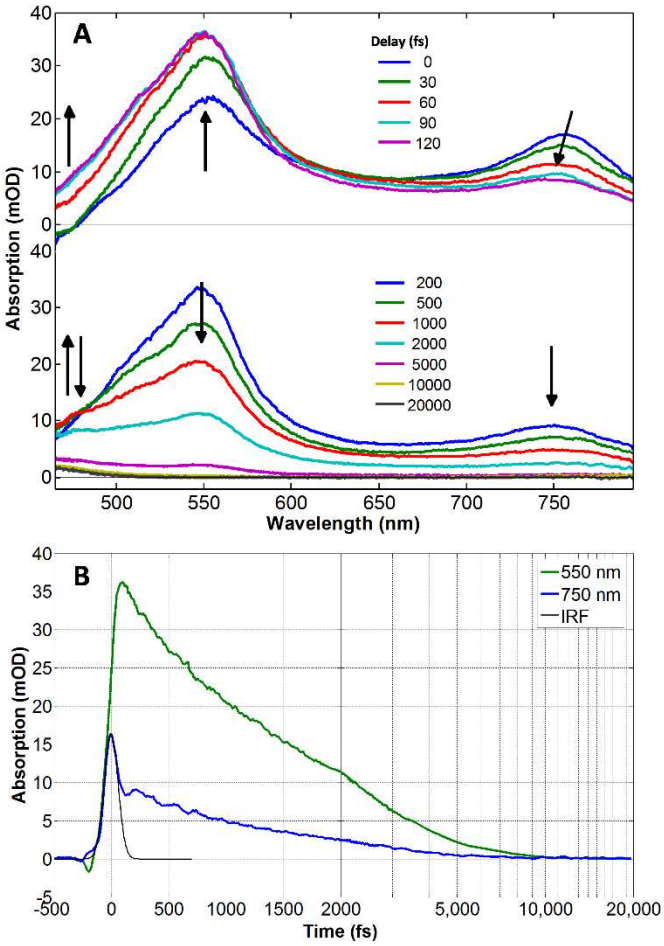

Figure 2. Ultrafast Transient Absorption. (A) TA spectra from 470 nm to 800 nm showing fast decay/rise of the bright/dark state on a 100 fs timescale, followed by a common population decay time of 1.6±0.2 ps, leading ultimately to repopulation of the ground state and formation of the isomer **1b**, which absorbs at <500 nm. (B). The corresponding kinetics in the two transient bands; the early time coherent vibrational dynamics are all detailed in supporting information Details on the fitting and analysis, including vibronic coherences, are presented in SI4

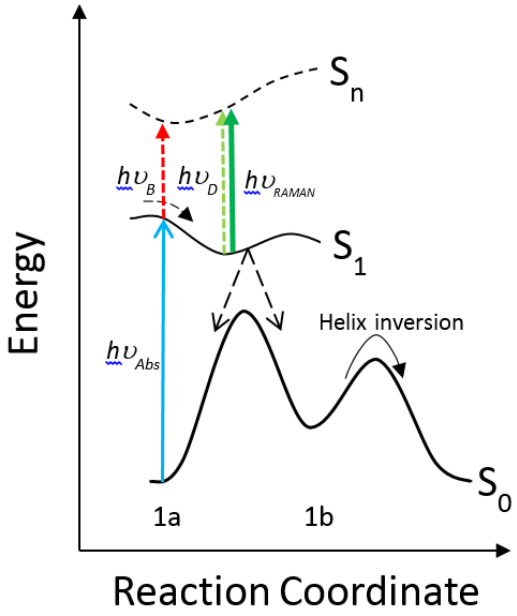

Figure 3. Schematic 1D plot of Energy as a Function of Reaction Coordinate. In this representation of the multidimensional reactive potential energy surface the Franck-Condon excited bright state absorbs at 760 nm. As structural relaxation occurs in 100 fs toward the dark state the S_1 energy decreases but the spectrum blue shifts, requiring increasing energy separation to S_n. The dark state is formed in 100 fs and absorbs at 550 nm. Its structure is significantly different to the bright state, such that the higher (S_n) excited state need not be of the same origin as for the bright state, and other intermediate states of lower transition moment may exist. As the dark state forms the S_0 energy increases and internal conversion to the ground state may occur at CIs. Note that the structural coordinate connecting bright and dark states need not be the same as that connecting the dark state to the CI and **1b**.

The coherently excited vibrational oscillations observed in time resolved fluorescence are also observed in the TA data (Figure 2B). The residual data recovered after subtraction of the 1.6 ps exponential fit were analysed in terms of a sum of damped cosine functions, with a sum of three functions required to obtain a good fit. The frequencies recovered were 114, 172 and 271 cm^{-1}, consistent with earlier fluorescence data.[20] The damping time constants have large errors

associated with them (SI S4) but a mean value of 530 fs is recovered. These coherently excited modes in the excited electronic state are most apparent in the bright state, but are also present in the dark state TA (Figs.2B, SI S6, S7). This is a significant result, showing that the vibronic coherences initially excited in the Franck-Condon bright state are preserved during the extensive structural reorganisation leading to the dark state. The correspondence between frequencies in the dark and bright states, and a mean damping time which is longer than the *ca* 100 fs required for light to dark conversion, suggests an assignment to 'spectator modes' i.e. modes that modulate the energy or transition moment of the excited state, but are not directly modified during the reaction. The persistence of such coherent vibrational dynamics into the dark state may have implications for the quantum yield of the isomerization, as recent simulations suggest that passage through a conical intersection is a function of vibrational coherence.[42]

For the FSRS measurements the 550 nm wavelength for the Raman pump (see experimental details) was chosen to be resonant with the S_1 to S_n transition of the dark state (Figure 3). Since the transition is strong (Figure 2A) the FSRS spectra will be dominated by resonantly enhanced Raman active modes of the dark state. The time dependent FSRS spectra (Figure 4A, B) are compared with the steady state stimulated Raman spectra of the **1a** ground state and with the long time (averaged over 70 - 100 ps) FSRS response shown in Fig. 4C. The latter measurement corresponds to a difference spectrum between the stimulated Raman spectra of the **1a** and **1b** ground states, but given that the red shifted absorption spectrum of **1b** (Fig. S9) is more strongly resonant with the Raman pump wavelength we expect its contribution to dominate the spectrum. The stimulated Raman spectrum for **1a** is in good agreement with the steady state resonance Raman spectrum (Fig. S10), as expected.

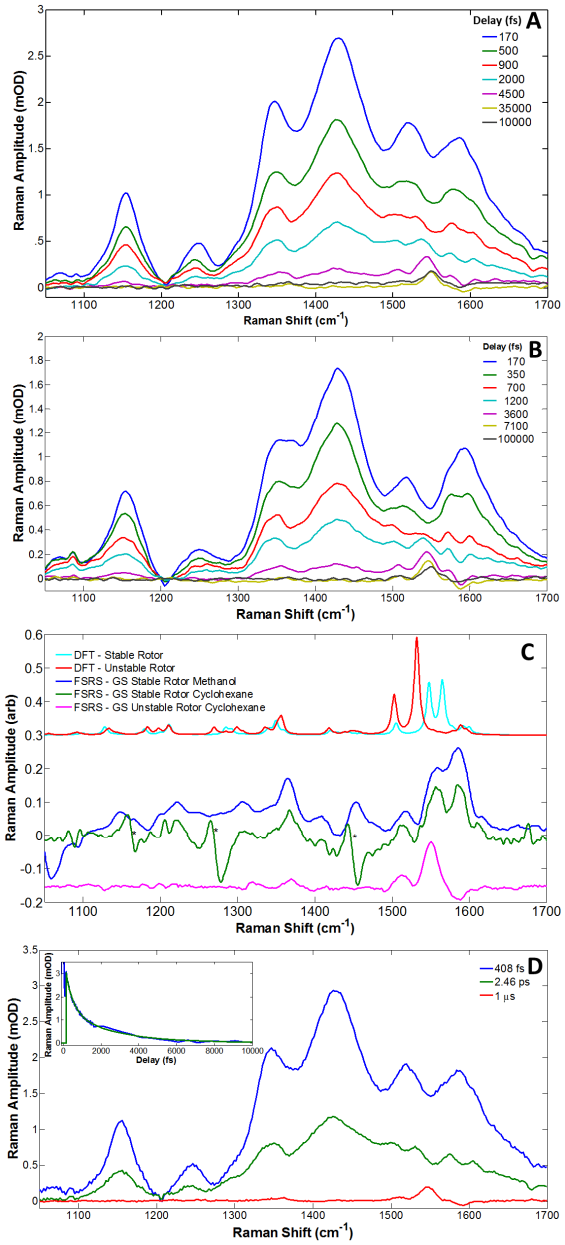

Figure 4. FSRS Data. The time dependent evolution of the FSRS data for excited **1a** in cyclohexane (A) and methanol(B) (C) The experimental stimulated Raman spectrum of **1a** in both solvents (blue methanol, green cyclohexane) is compared with the long-time FSRS spectrum (pink) and the DFT calculated Raman spectra for **1a** (cyan) and **1b** (red). (D) EAS recovered through a double exponential global analysis of the FSRS data in (A); the quality of fit is shown inset. Complete details of the data analysis are presented in SI9 figures S13-15

These experimental ground state spectra are complemented by DFT calculations for **1a** and **1b**, (Fig. 4C). There is good agreement between calculation and experiment. The Raman spectrum of **1a** is dominated by two broad modes around 1580 cm^{-1} matching the intense pair of calculated modes. The experiment suggests a red shift for the most Raman active modes between **1a** and **1b**, which is again reproduced in the calculation. The DFT calculations reveal that for both **1a** and **1b** the cluster of modes around 1400 - 1700 cm^{-1} arise mainly from C=C stretches, with the most intense (for **1a** calculated at 1564 and 1547 cm^{-1} and for **1b** red-shifted at 1532 and 1503 cm^{-1}) having major contributions from the stretch of the olefinic bridging bond; detailed DFT assignments are presented in supporting information (Table S1) and the bond displacements for the five most Raman active modes of **1a** and **1b** are shown in Fig S5. A major contribution from bridge localised modes in the resonance Raman spectrum suggests that such modes are displaced in the transition between the ground and bright states. DFT calculations of the HOMO and LUMO for **1a** are shown in Figure 5. It is apparent that the excitation is localised on the C=C bond, and that HOMO and LUMO are bonding and anti-bonding with respect to electronic excitation. This is wholly consistent with both the Raman enhancements and a reduced bond order in the excited state leading to the twisting and pyramidalization reported in calculations.

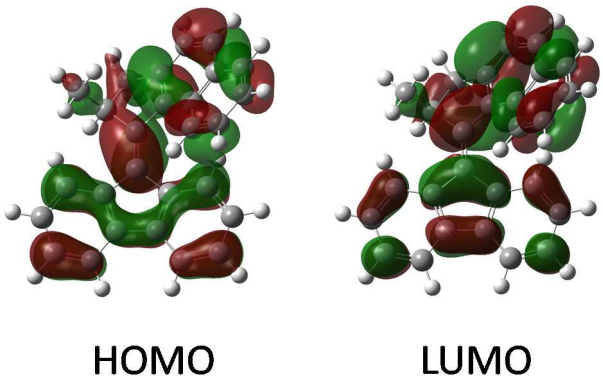

Figure 5. DFT Calculation The HOMO and LUMO from the DFT calculation (SI S3) showing localisation of excitation on the bridging bond.

The FSRS signals beyond 170 fs decay monotonically (Fig. 4A). The 100 fs rise resolved in TA is not recovered, as the first 170 fs of data are obscured by a coherence artefact during pulse overlap. FSRS experiments were conducted in both polar H-bonding methanol and nonpolar cyclohexane which yielded very similar spectra (Fig 4A,B) and kinetics. This suggests that intramolecular electronic and nuclear structure relaxation dominate the excited state dynamics, and the medium has only a minor effect on dark state structure.

The FSRS decay is non-single exponential (see below), but the mean time constant (1.4 ps) is in accord with that for TA decay (1.6 ps). This confirms the assignment of the FSRS to the dark state. The most intense FSRS signals are observed at 1430 and 1345 cm^{-1} (Figure 4A), markedly red shifted with respect to the most intense experimental ground state Raman bands (1585 and 1560 cm^{-1}, Figure 4B). Similar but smaller red shifts were noted in studies of the "stiff-stilbene" photoisomerization, which also proceeds following excitation localised on a bridging C=C bond.[43] The 70 cm^{-1} red shift in that case was associated with a calculated lengthening of the ethylenic bond by 7 pm. The larger red shift seen here suggests an even larger change in **1a** structure; such large shifts are consistent with the results of theoretical calculation. For example, Filatov calculated that the bridging bond extends by 13 pm between ground state and the lowest energy CI in an earlier generation alkene based molecular motor.[18] A similarly large extension of an ethylenic bond was calculated upon excitation of diphenyl dibenzofulvene.[44] The red shift in the dominant modes detected in FSRS is thus interpreted as reflecting localisation of the $S_0 \rightarrow S_1$ excitation on the olefinic bridging bond (Fig. 5), leading to reduced bond order in the Franck-Condon excited state, which in-turn allows the structural evolution (pyramidalization and twisting[18-19]) to form the dark state structure, which has a significantly extended bridging bond compared to the ground state.

An alternative explanation for the red shift is that higher quanta of the C=C stretch are populated in the Franck Condon state, and retain their population in the dark state. In that case the FSRS spectra may reflect a 'hot band' Raman transition from v = 1 to 2, thus red shifted due to the anharmonicity.

This is a less likely explanation, as the C=C stretch plays a major role in the electronic transition and is thus strongly perturbed upon excitation, undergoing a large frequency shift. Further, the bridging C=C bond is intimately involved in the highly anharmonic reaction coordinate (twisting, stretching and pyramidalization). Both of these factors will contribute to very strong coupling with low frequency background modes and ultrafast intramolecular vibrational relaxation (IVR) will occur for any population initially in the C=C stretch.

Two other features of the FSRS spectra deserve comment. The Raman linewidths in the excited state (Fig. 4A,B) are on the order of 50 cm^{-1}, significantly broader than those measured in the ground state (Fig. 4C), the widths of which mainly reflect the instrumental resolution. The broad linewidth can in part be ascribed to lifetime broadening, with the 1.5 ps lifetime yielding a line width of ca 15 cm^{-1}. In addition, as noted above (Fig. 3), the dark state is formed rapidly in an energetically downhill process. Thus the dark state is expected to have considerable excess energy residing, after rapid IVR, in low frequency modes. Coupling between this hot vibrational distribution and the higher frequency stretch modes probed in FSRS will also contribute to an increased linewidth. The second noteworthy feature is that a significantly larger number of modes contribute to the excited state Raman spectra than appear in the ground state. The appearance of numerous Raman active modes is not in itself surprising. The ground state DFT calculation reveals numerous modes in this region, largely associated with C=C stretches localised on the fluorene and naphthyl rings of **1a** (SI3, Table S1). We assign the difference between the sparse ground state and rich excited state spectra observed here to the dominance of the bridge C=C stretch in the S_0-S_1 resonance enhanced spectrum, arising from the expected large displacement (Fig. 5). The FSRS spectrum on the other hand is resonant with S_1 to S_n, and thus need not show the same enhancement pattern. The detailed assignment of the FSRS spectrum therefore requires both high quality calculations of the dark state spectrum, and further experiments with isotopically labelled samples; progress in this direction is encouraging.[25]

One further possible origin of additional modes in FSRS is a contribution from the S_n state, arising from coherence Stokes Raman scattering (CSRS). Ernsting et al recently showed the appearance of S_1 vibrations in broadband CSRS measurements resonant with $S_0 \rightarrow S_1$ transition.[45] This seems less likely here as the inherently ultrafast lifetime of higher excited S_n states will make any such contribution extremely broad and thus difficult to resolve.

Significantly, the shape of the FSRS spectrum evolves over time (Figure 4A). In particular the pair of higher frequency modes at 1590 and 1520 cm^{-1} are well resolved at 170 fs but ill-defined by 1 ps. The evolution persists for ca 10 ps when the final state is formed. The final state (time averaged spectrum in Figure 4C) is readily identified as **1b** by a comparison with the calculated Raman spectrum (see below). Thus to a first approximation the spectral evolution can be considered simply as decay of the dark state to form **1b** (and **1a**), where the formation of **1b** yields the mode at ca. 1560 cm^{-1} which 'fills in' the intensity between the 1590/1520 cm^{-1} pair. Such a mechanism predicts an evolution with a single time constant and single final species, **1b**. The FSRS were analysed using a global analysis procedure assuming this model, and the evolution associated spectra (EAS) are presented in Fig. S13b. While qualitatively satisfactory the single exponential fit does not adequately describe the data; for example the deviation between experimental and fitted intensities around 2-4 ps at 1430 cm^{-1} is apparent. Secondly the recovered time constant is 1 ps, which is less than the 1.6 ps dark state decay time measured accurately in TA. Finally, the long-time 'final' spectrum has a non-physical sloping baseline that does not correspond to **1b** (Figure 4BC). Consequently we added an additional component to the global analysis. In that case the fit is good (Fig. S16), the mean decay time reflects the time constant recovered from the TA and the final spectrum has a flat baseline. Essentially the same results as in Fig 4 d were obtained for methanol (Fig. S13, S14).

The global analysis shows the FSRS relaxing in 400 fs to an intermediate spectrum which already contains part of the **1b** spectrum but is otherwise similar to the early time spectrum. We suggest that the origin of the non-single exponential decay of the dark state lies in its ultrafast formation.

Being formed in ca 100 fs the initial dark state will appear with a nonthermal population in low frequency modes which will depend on the initial excitation energy and the intramolecular coupling. On a picosecond timescale this population evolves, leading to different mode coupling patterns which will in turn modify the high frequency spectra observed in Fig. 4. Similar spectral evolution has been seen in other systems by FSRS.[46] There is no reason to expect *a priori* such an intramolecular relaxation to be governed by an exponential decay law, so the intermediate EAS simply reflects a continuous evolution of the dark state spectrum, and it is this spectral evolution which lends the FSRS a nonexponential relaxation while the dark state population decay kinetics are monoexponential.

A second important feature of the FSRS is the long lived (permanent on the 100 picosecond timescale) pair of transitions at 1550 and 1510 cm^{-1}. As mentioned above, these are assigned to vibrational modes of the metastable **1b** form, even though **1b** is not fully resonant with the Raman pump (Fig. S9). Since FSRS records the difference spectrum, these transitions, if they are from **1b**, must arise from a vibrational mode which is shifted with respect to **1a**. The DFT calculation indeed predicts two such shifted modes with significant Raman amplitude and contributions from the olefinic C=C stretch (Fig. 4C, SI S5); this is consistent with an assignment of the long lived FSRS to **1b**. These data thus show that **1b** forms directly from the dark state. We further note a slow (tens of picoseconds) shift of the **1b** mode to higher frequency (Fig. 4A), which we ascribe to excess energy in S_0, which is formed with a high vibrational temperature by isoenergetic internal conversion from the S_1 dark state. The initially formed hot ground state will relax by IVR to populate a distribution of low frequency modes. The effect of anharmonic coupling of these low frequency modes to the C=C stretch is to shift the Raman active mode to lower wavenumber.[47] As the low frequency modes transfer energy to the solvent on a picosecond time scale the C=C mode shifts to higher wavenumber, as observed.

Finally we note the occurrence of a weak and persistent negative signal at 1590 cm^{-1}. A long-lived negative feature is not expected from the $S_1 \rightarrow S_n$ resonance used to generate the FSRS. Such features have been observed in other FSRS experiments[41, 48] and may reflect the appearance of dispersive lineshapes[48]. However, we note that this negative signal matches closely the most intense ground state feature in the Raman spectrum. There are additional (albeit non-resonant) pathways through which the ground state could contribute to the FSRS spectrum.[41] Consequently, the possibility of ground state modes contributing even in the fully resonant $S_1 \rightarrow S_n$ FSRS spectrum is a complicating feature which should be borne in mind when analysing such data.

Conclusion

We have investigated excited state dynamics of the best established light driven molecular motor. Both ultrafast population dynamics and the vibrational structure of an intermediate dark excited electronic state in the photocycle have been characterized. The bright Franck-Condon excited state decays in <100 fs to establish an equilibrium with the dark state. This excited state structure change is accompanied by coherent excitation of vibrational modes. The vibrational coherences are attenuated in the dark state but nevertheless survive the 100 fs structural evolution from the bright state. The dark state spectrum is characterized by a marked decrease in the frequency of Raman active modes. This is assigned to elongation and weakening of the bridging olefinic bond. Other C=C ring-localised modes are resolved in the dark state with greater amplitude compared to the ground electronic state, due to a change in the resonance condition. Further intramolecular relaxation was observed in the dark state through evolution of the FSRS spectral profile. The excited dark state population decays directly back to the ground electronic state in 1.6 ps, partitioning between the original (**1a**) and metastable (**1b**) forms. The photochemical product **1b** is formed from the dark state with considerable excess vibrational energy. This excess energy relaxes via ultrafast IVR and subsequently cools by energy transfer to the solvent on the tens of picoseconds timescale.

Experimental Details. The synthesis and characterization of **1a** has been described elsewhere.[11] Measurements were made in a 0.2 mm cuvette with an OD of 0.4; excitation was at 390 nm. The laser source is detailed elsewhere.[49] The spectrometers used for TA and FSRS and the measurement and signal processing procedures are detailed in supporting information. The global analysis software used has been described elsewhere.[50]

Acknowledgements. SRM is grateful to EPSRC for financial support (EP/J009148/01, EP/M00197/1) and BLF thanks the ERC (Advanced Investigator Grant 227897). JF thanks EPSRC for the award of a studentship. The calculations presented in this paper were carried out on the High Performance Computing Cluster supported by the Research and Specialist Computing Support service at the University of East Anglia.

References

1. Kinbara, K.; Aida, T., Toward Intelligent Molecular Machines: Directed Motions of Biological and Artificial Molecules and Assemblies. *Chem. Rev.***2005,** *105* (4), 1377-1400.
2. Balzani, V.; Credi, A.; Venturi, M., Light powered molecular machines. *Chem. Soc. Rev.* **2009,** *38* (6), 1542-1550.
3. Perez-Hernandez, G.; Pelzer, A.; Gonzalez, L.; Seideman, T., Biologically inspired molecular machines driven by light. Optimal control of a unidirectional rotor. *New J. Phys.* **2010,** *12*, 24.
4. Feringa, B. L., In control of motion: From molecular switches to molecular motors. *Acc. Chem. Research* **2001,** *34* (6), 504-513.
5. Kay, E. R.; Leigh, D. A.; Zerbetto, F., Synthetic molecular motors and mechanical machines. *Angew. Chem.-Int. Ed.* **2007,** *46* (1-2), 72-191.
6. Feringa, B. L., The art of building small: From molecular switches to molecular motors. *J. Org. Chem.* **2007,** *72* (18), 6635-6652.
7. Pollard, M. M.; Klok, M.; Pijper, D.; Feringa, B. L., Rate acceleration of light-driven rotary molecular motors. *Adv. Functional Mat.* **2007,** *17* (5), 718-729.
8. Vicario, J.; Meetsma, A.; Feringa, B. L., Controlling the speed of rotation in molecular motors. Dramatic acceleration of the rotary motion by structural modification. *Chem. Comm.* **2005,** (47), 5910-5912.
9. Klok, M.; Browne, W. R.; Feringa, B. L., Kinetic analysis of the rotation rate of light-driven unidirectional molecular motors. *Phys. Chem. Chem. Phys.* **2009,** *11* (40), 9124-9131.
10. Klok, M.; Janssen, L.; Browne, W. R.; Feringa, B. L., The influence of viscosity on the functioning of molecular motors. *Faraday Disc.* **2009,** *143*, 319-334.
11. Pollard, M. M.; Meetsma, A.; Feringa, B. L., A redesign of light-driven rotary molecular motors. *Org. Biomol. Chem.* **2008,** *6* (3), 507-512.
12. Pollard, M. M.; Wesenhagen, P. V.; Pijper, D.; Feringa, B. L., On the effect of donor and acceptor substituents on the behaviour of light-driven rotary molecular motors. *Org. Biomol. Chem* **2008,** *6* (9), 1605-1612.
13. Kistemaker, J. C. M.; Stacko, P.; Visser, J.; Feringa, B. L., Unidirectional rotary motion in achiral molecular motors. *Nature Chem.* **2015,** *7* (11), 890-896.
14. van Delden, R. A.; ter Wiel, M. K. J.; Pollard, M. M.; Vicario, J.; Koumura, N.; Feringa, B. L., Unidirectional molecular motor on a gold surface. *Nature* **2005,** *437* (7063), 1337-1340.
15. van Delden, R. A.; Koumura, N.; Harada, N.; Feringa, B. L., Unidirectional rotary motion in a liquid crystalline environment: Color tuning by a molecular motor. *Proc. Nat. Acad. Sci. USA* **2002,** *99* (8), 4945-4949.
16. Eelkema, R.; Pollard, M. M.; Vicario, J.; Katsonis, N.; Ramon, B. S.; Bastiaansen, C. W. M.; Broer, D. J.; Feringa, B. L., Nanomotor rotates microscale objects. *Nature* **2006,** *440* (7081), 163-163.
17. Kudernac, T.; Ruangsupapichat, N.; Parschau, M.; Macia, B.; Katsonis, N.; Harutyunyan, S. R.; Ernst, K. H.; Feringa, B. L., Electrically driven directional motion of a four-wheeled molecule on a metal surface. *Nature* **2011,** *479* (7372), 208-211.
18. Kazaryan, A.; Kistemaker, J. C. M.; Schafer, L. V.; Browne, W. R.; Feringa, B. L.; Filatov, M., Understanding the Dynamics Behind the Photoisomerization of a Light-Driven Fluorene Molecular Rotary Motor. *J. Phys. Chem. A* **2010,** *114* (15), 5058-5067.
19. Kazaryan, A.; Lan, Z.; Schafer, L. V.; Thiel, W.; Filatov, M., Surface Hopping Excited-State Dynamics Study of the Photoisomerization of a Light-Driven Fluorene Molecular Rotary Motor. *J. Chem. Theory Comp.* **2011,** *7* (7), 2189-2199.
20. Conyard, J.; Addison, K.; Heisler, I. A.; Cnossen, A.; Browne, W. R.; Feringa, B. L.; Meech, S. R., Ultrafast dynamics in the power stroke of a molecular rotary motor. *Nature Chem.* **2012,** *4* (7), 547-551.
21. Conyard, J.; Cnossen, A.; Browne, W. R.; Feringa, B. L.; Meech, S. R., Chemically Optimizing Operational Efficiency of Molecular Rotary Motors. *J. Amer. Chem. Soc.* **2014,** *136* (27), 9692-9700.

22. Oruganti, B.; Wang, J.; Durbeej, B., Computational Insight to Improve the Thermal Isomerisation Performance of Overcrowded Alkene-Based Molecular Motors through Structural Redesign. *Chemphyschem* **2016,** *17* (21), 3399-3408.
23. Nikiforov, A.; Gamez, J. A.; Thiel, W.; Filatov, M., Computational Design of a Family of Light-Driven Rotary Molecular Motors with Improved Quantum Efficiency. *J. Phys. Chem Letters* **2016,** *7* (1), 105-110.
24. Hu, M. X.; Xu, T.; Momen, R.; Huan, G.; Kirk, S. R.; Jenkins, S.; Filatov, M., A QTAIM and Stress Tensor Investigation of the Torsion Path of a Light-Driven Fluorene Molecular Rotary Motor. *J. of Comp. Chem.* **2016,** *37* (29), 2588-2596.
25. Amirjalayer, S.; Cnossen, A.; Browne, W. R.; Feringa, B. L.; Buma, W. J.; Woutersen, S., Direct Observation of a Dark State in the Photocycle of a Light-Driven Molecular Motor. *J. Phys. Chem A* **2016,** *120* (43), 8606-8612.
26. Filatov, M.; Olivucci, M., Designing Conical Intersections for Light-Driven Single Molecule Rotary Motors: From Precessional to Axial Motion. *J Org. Chem.* **2014,** *79* (8), 3587-3600.
27. Amatatsu, Y., Theoretical Study of Topographical Features around the Conical Intersections of 9-(2-Cyclopenten-1-ylidene)-9H-fluorene. *J. Phys. Chem A* **2013,** *117* (47), 12529-12539.
28. Pang, X.; Cui, X.; Hu, D.; Jiang, C.; Zhao, D.; Lan, Z.; Li, F., "Watching" the Dark State in Ultrafast Nonadiabatic Photoisomerization Process of a Light-Driven Molecular Rotary Motor. *J. Phys. Chem A* **2017,** *121*, 1240-1249.
29. Greb, L.; Lehn, J. M., Light-Driven Molecular Motors: lmines as Four-Step or Two-Step Unidirectional Rotors. *J. Amer. Chem. Soc.* **2014,** *136* (38), 13114-13117.
30. Amatatsu, Y., Computational Design of a Fluorene-Based Ethylenoid Bridged by Trimethylene Chain. *Bull. Chem. Soc. Japan* **2016,** *89* (10), 1245-1259.
31. Hall, C. R.; Conyard, J.; Laptenok, S.; Browne, W.; Feringa, B.; Heisler, I.; Meech, S. In *Ultrafast Isomerization Dynamics of a Unidirectional Molecular Rotor Revealed by Femtosecond Stimulated Raman Spectroscopy (FSRS)*, International Conference on Ultrafast Phenomena, Santa Fe, New Mexico, 2016/07/17; Optical Society of America: Santa Fe, New Mexico, 2016; p UM2A.3.
32. Wang, Y. L.; Tang, L. T.; Liu, W. M.; Zhao, Y. X.; Oscar, B. G.; Campbell, R. E.; Fang, C., Excited State Structural Events of a Dual-Emission Fluorescent Protein Biosensor for Ca2+ Imaging Studied by Femtosecond Stimulated Raman Spectroscopy. *J. Phys. Chem. B* **2015,** *119* (6), 2204-2218.
33. Kukura, P.; McCamant, D. W.; Mathies, R. A., Femtosecond stimulated Raman spectroscopy. In *Annual Review of Physical Chemistry*, 2007; Vol. 58, pp 461-488.
34. Dasgupta, J.; Frontiera, R. R.; Taylor, K. C.; Lagarias, J. C.; Mathies, R. A., Ultrafast excited-state isomerization in phytochrome revealed by femtosecond stimulated Raman spectroscopy. *Proc. Nat. Acad. Sci. USA* **2009,** *106* (6), 1784-1789.
35. Fang, C.; Frontiera, R. R.; Tran, R.; Mathies, R. A., Mapping GFP structure evolution during proton transfer with femtosecond Raman spectroscopy. *Nature* **2009,** *462* (7270), 200-U74.
36. Fujisawa, T.; Kuramochi, H.; Hosoi, H.; Takeuchi, S.; Tahara, T., Role of Coherent Low-Frequency Motion in Excited-State Proton Transfer of Green Fluorescent Protein Studied by Time-Resolved Impulsive Stimulated Raman Spectroscopy *J. Amer. Chem. Soc.* **2016,** *138* (12), 3942-3945.
37. Takeuchi, S.; Tahara, T., Coherent nuclear wavepacket motions in ultrafast excited-state intramolecular proton transfer: Sub-30-fs resolved pump-probe absorption spectroscopy of 10-hydroxybenzo h quinoline in solution. *J. Phys. Chem A* **2005,** *109* (45), 10199-10207.
38. Takeuchi, S.; Ruhman, S.; Tsuneda, T.; Chiba, M.; Taketsugu, T.; Tahara, T., Spectroscopic Tracking of Structural Evolution in Ultrafast Stilbene Photoisomerization. *Science* **2008,** *322* (5904), 1073-1077.
39. Wende, T.; Liebel, M.; Schnedermann, C.; Pethick, R. J.; Kukura, P., Population-Controlled Impulsive Vibrational Spectroscopy: Background- and Baseline-Free Raman Spectroscopy of Excited Electronic States. *J. Phys. Chem A* **2014,** *118* (43), 9976-9984.

40. Schnedermann, C.; Liebel, M.; Kukura, P., Mode-Specificity of Vibrationally Coherent Internal Conversion in Rhodopsin during the Primary Visual Event. *J. Amer. Chem. Soc.* **2015,** *137* (8), 2886-2891.
41. Weigel, A.; Dobryakov, A.; Klaumunzer, B.; Sajadi, M.; Saalfrank, P.; Ernsting, N. P., Femtosecond Stimulated Raman Spectroscopy of Flavin after Optical Excitation. *J. Phys. Chem. B* **2011,** *115* (13), 3656-3680.
42. Duan, H.-G.; Miller, R. J. D.; Thorwart, M., Impact of Vibrational Coherence on the Quantum Yield at a Conical Intersection. *J. Phys. Chem Letts* **2016,** *7* (17), 3491-3496.
43. Quick, M.; Berndt, F.; Dobryakov, A. L.; Ioffe, I. N.; Granovsky, A. A.; Knie, C.; Mahrwald, R.; Lenoir, D.; Ernsting, N. P.; Kovalenko, S. A., Photoisomerization Dynamics of Stiff-Stilbene in Solution. *J. Phys. Chem. B* **2014,** *118* (5), 1389-1402.
44. Li, Q. S.; Blancafort, L., A conical intersection model to explain aggregation induced emission in diphenyl dibenzofulvene. *Chem. Comm.* **2013,** *49* (53), 5966-5968.
45. Quick, M.; Dobryakov, A. L.; Kovalenko, S. A.; Ernsting, N. P., Resonance Femtosecond-Stimulated Raman Spectroscopy without Actinic Excitation Showing Low-Frequency Vibrational Activity in the S-2 State of All-Trans beta-Carotene. *J. Phys. Chem Letters* **2015,** *6* (7), 1216-1220.
46. Ruchira Silva, W.; Frontiera, R. R., Excited state structural evolution during charge-transfer reactions in betaine-30. *Phys. Chem. Chem. Phys.* **2016,** *18* (30), 20290-20297.
47. Nakabayashi, T.; Okamoto, H.; Tasumi, M., Probe-Wavelength Dependence of Picosecond Time-Resolved Anti-Stokes Raman Spectrum of Canthaxanthin: Determination of Energy States of Vibrationally Excited Molecules Generated via Internal Conversion from the Lowest Excited Singlet State. *J. Phys. Chem A* **1997,** *101* (19), 3494-3500.
48. Brown, K. E.; Veldkamp, B. S.; Co, D. T.; Wasielewski, M. R., Vibrational Dynamics of a Perylene-Perylenediimide Donor-Acceptor Dyad Probed with Femtosecond Stimulated Raman Spectroscopy. *J. Phys. Chem Letters* **2012,** *3* (17), 2362-2366.
49. Heisler, I. A.; Moca, R.; Camargo, F. V. A.; Meech, S. R., Two-dimensional electronic spectroscopy based on conventional optics and fast dual chopper data acquisition. *Review of Scientific Instruments* **2014,** *85* (6).
50. Snellenburg, J. J.; Laptenok, S. P.; Seger, R.; Mullen, K. M.; van Stokkum, I. H. M., Glotaran: A Java-Based Graphical User Interface for the R Package TIMP. *J. Statistical Software* **2012,** *49* (3), 1-22.

ToC Graphic